Effect of Turbulence Models on Simulated Iced Aircraft Airfoil

Muhammad Afzal, Cao Yihua, Zhao Ming

Abstract—The present work describes a computational study of aerodynamic characteristics of GLC305 airfoil clean and with 16.7 min ice shape (rime 212) and 22.5 min ice shape (glaze 944).The performance of turbulence models SA, Kε, Kω Std, and Kω SST model are observed against experimental flow fields at different Mach numbers 0.12, 0.21, 0.28 in a range of Reynolds numbers $3x10^6$, $6x10^6$, and $10.5x10^6$ on clean and iced aircraft airfoil GLC305. Numerical predictions include lift, drag and pitching moment coefficients at different Mach numbers and at different angle of attacks were done. Accuracy of solutions with respect to the effects of turbulence models, variation of Mach number, initial conditions, grid resolution and grid spacing near the wall made the study much sensitive. Navier Stokes equation based computational technique is used. Results are very close to the experimental results. It has seen that SA and SST models are more efficient than Kε and Kω standard in under study problem.

Keywords—Aerodynamics, Airfoil GLC305, Iced Airfoil, Turbulence Model

I. INTRODUCTION

ICING on aircraft during flight has being remain hazardous. It destroys the smooth flow of air, increasing drag while decreasing the ability of the airfoil to create lift. To maintain altitude and counter the effects of drag during flight in icing conditions, the angle of attack (AOA) is generally increased and more power is applied to the engine(s). On December 27, 1968 first jet air transport accident linked to airframe icing occurred.[1] Therefore it became more important to study the icing effect on aircraft. The effect of ice accumulated on aircraft can be study through flight tests, wind tunnel measurements and computational fluid dynamics (CFD) simulations. First two methods are comparatively expensive than 3rd one i.e. CFD. Computational Fluid Dynamics has grown from an art and mathematical curiosity to become an essential tool in almost every branch of fluid dynamics and aerodynamics.

Generation of high quality structured grids for iced airfoils is a great challenge. Chi, et al[2] presented single and multi-block structured grid for much complicated iced shapes airfoils. It was observed that multi block grid take much time to converge.

Afzal M. is MS student in Beijing Aeronautics and Aestronautics University, Beijing, China(phone: +86-1355-292-4984;e-mail: mafzalmgr@yahoo.co.uk).

Yihua C. He is working as professor in Beijing Aeronautics and Aestronautics University, Beijing, China, (phone: +86-1368-149-1896; email:yihuacaocs@yahoo.com.cn).

Ming Z. is doctoral candidate in Beijing Aeronautics and Aestronautics University,Beijing,P.R.China,(phone:+86-1381-181-4671; zmbuaa@163.com)

II. OBJECTIVE

The objective of this study is to evaluate the accuracy and validation of turbulence models SA, k-ω standard, k-ω SST and k-ε in Navier – Stoke equation based solver for iced aircraft airfoils at low Mach numbers and high Reynolds numbers. Secondly, compute aerodynamic characteristics in icing conditions.

III. PROBLEM DESCRIPTION

In this study, a business aircraft airfoil GLC305[3] with 16.7 minute rime ice shape 212 and 22.5 minute glaze ice shape 944 of two large protruding horns are selected. The flow fields around these iced airfoils are sufficiently complex. For the accuracy of the CFD predictions, experimental data of NASA Glenn's Icing Research Tunnel is used as ref. [4] Rime ice is formed when small supercooled water droplets freeze on contact with a sub-zero surface. Because the droplets are small, they freeze almost instantly creating a mixture of tiny ice particles and trapped air. The ice deposit formed is rough and crystalline and opaque. High sensitive meshes generated around clean and iced airfoils.Flow fields at three Mach numbers 0.12, 0.21 and 0.28 for high Reynolds number $3x10^6$, $6x10^6$, and $10.5x10^6$ are investigated.
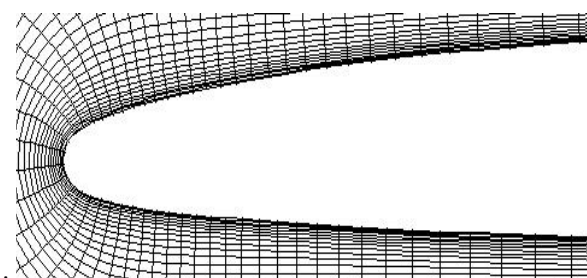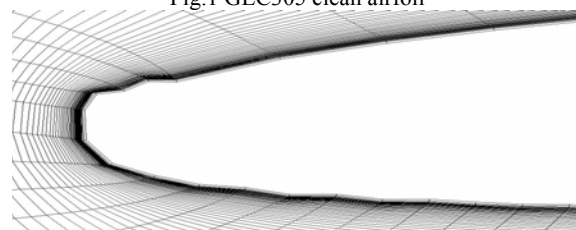

Fig.1 GLC305 clean airfoil

Fig.2 GLC305 airfoil with rime 212 ice shape

World Academy of Science, Engineering and Technology
International Journal of Aerospace and Mechanical Engineering
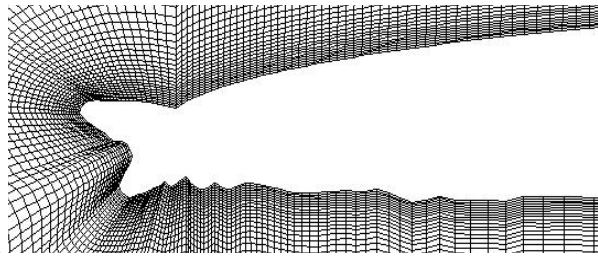Vol:5, No:8, 2011

Fig.3 GLC305 airfoil with glaze 944 ice shape

IV. FORMULATION AND NUMERICAL METHOD OF SOLUTION

Navier-Stoke equation based code was used to solve iced-airfoil problem. General form of the conservation law for scalar quantity U is given as

$$\frac{\partial}{\partial t}\int_{\Omega} U d\Omega + \oiint_{\partial\Omega}\left[U(\vec{v}.\vec{n}) - \kappa_\rho(\nabla U^*.\vec{n})\right]ds$$
$$= \int_{\Omega} Q_v d\Omega + \oiint_{\partial\Omega}(\overrightarrow{Q_S}.\vec{n})ds \tag{1}$$

Where $U^* = U/\rho$ and k is the thermal diffusivity coefficient. The convective and diffusive flux would become tensors instead of vectors - $\overline{F_C}$ the convective flux tensor and - $\overline{F_D}$ the diffusive flux tensor. The volume sources would be a vector. $\overline{Q_v}$ and $\overline{Q_S}$ would change into tensor $\overline{Q_s}$.

$$\frac{\partial}{\partial t}\int_{\Omega}\vec{U} d\Omega + \oiint_{\partial\Omega}\left[(\overline{\overline{F_C}} - \overline{\overline{F_D}}).\vec{n}\right]ds$$
$$= \int_{\Omega}\overline{Q_v} d\Omega + \oiint_{\partial\Omega}(\overline{\overline{Q_S}}.\vec{n})ds \tag{2}$$

The time rate of change of the total mass inside the finite volume Ω is equal to product of density, surface area and velocity component perpendicular to surface. [5] Momentum conservation inside an arbitrary control volume Ω which is fixed in space as

$$\frac{\partial}{\partial t}\int_{\Omega}\rho\vec{v} d\Omega + \oiint_{\partial\Omega}\rho\vec{v}(\vec{v}.\vec{n})dS$$
$$= \int_{\Omega}\rho\vec{f_e} d\Omega - \oiint_{\partial\Omega} p\vec{n}dS + \oiint_{\partial\Omega}(\overline{\overline{\tau}}.\vec{n})dS \tag{3}$$

And energy conservation equation is

$$\frac{\partial}{\partial t}\int_{\Omega}\rho E d\Omega + \oiint_{\partial\Omega}\rho E(\vec{v}.\vec{n})dS = \oiint_{\partial\Omega}\kappa(\nabla T.\vec{n})dS$$
$$+ \int_{\Omega}(\rho\vec{f_e}.\vec{v} + \dot{q}h)d\Omega - \oiint_{\partial\Omega} p(\vec{v}.\vec{n})dS + \oiint_{\partial\Omega}(\overline{\overline{\tau}}.\vec{v}).\vec{n}dS \tag{4}$$

In aerodynamics, working fluid behaves like a calorically perfect gas whose equation of state assumes the form [6], [7]

$$p = \rho R T$$
$$R = c_p - c_v, \gamma = \frac{c_p}{c_v}, h = c_p T \tag{5}$$
$$p = (\gamma - 1)\rho\left[E - \frac{u^2 + v^2 + w^2}{2}\right]$$

The viscosity of a fluid relates to the transport of momentum in the direction of velocity gradient. The coefficient of the dynamic viscosity is a function of temperature and pressure. For a perfect gas, μ strongly dependent on temperature but weakly dependent on pressure. [8] Sutherland formula (in SI units)

$$\mu = \frac{1.45 T^{3/2}}{T + 110}.10^{-6} \tag{6}$$

The temperature T is in degree Kelvin (K), at T= 288 K, μ= 1.78x10^{-5}kg/ms

Structure and unstructured types meshes in NS equation based codes are used normally. Here structure grids are generated on clean and iced shape GLC305 airfoil because it saves the time of simulation. A control volume based technique consists of integrating the governing equations about each control volume, yielding discrete equations that conserve each quantity. The flow property values are stored at the cell centre. The face value, which is needed for the element flux integration, is derived from the cell centre value. A second-order upwind scheme was applied in the computation for clean airfoil flows, while both first-order and second-order solvers were used for the iced airfoil cases. When the first-order upwind scheme is employed, this value is simply taken from its upwind cell. For 2nd order upwind scheme,

$$\phi_f = \phi + \nabla \bullet \Delta S \tag{7}$$

Where $\varphi_f = \varphi + \nabla\varphi\bullet\Delta S$
The gradient of function in discrete form is

$$\nabla\phi = \frac{1}{A}\iint\nabla\phi\bullet dS = \frac{1}{A}\int\phi\bullet d\vec{L} = \frac{1}{A}\sum_f^{Nforces}\tilde{\phi}_f\vec{L} \tag{8}$$

V. TURBULENCE MODELS

Navier-Stokes equation in differential form

$$\frac{\partial}{\partial t}\int_{\Omega}\vec{W} d\Omega + \oiint_{\partial\Omega}(\vec{F_c} - \vec{F_v})ds = \int_{\Omega}\vec{Q} d\Omega \tag{9}$$

In the absence of source terms in coordinate invariant, for compressible Newtonian fluid

$$\frac{\partial\rho}{\partial t} + \frac{\partial}{\partial x_i}(\rho\upsilon_i) = 0$$
$$\frac{\partial}{\partial t}(\rho\upsilon_i) + \frac{\partial}{\partial x_i}(\rho\upsilon_j\upsilon_i) = -\frac{\partial p}{\partial x_i} + \frac{\partial\tau_{ij}}{\partial x_j} \tag{10}$$
$$\frac{\partial}{\partial t}(\rho E) + \frac{\partial}{\partial x_j}(\rho\upsilon_j H) = \frac{\partial}{\partial x_j}(\upsilon_i\tau_{ij}) + \frac{\partial}{\partial x_j}(k\frac{\partial T}{\partial x_j})$$

υ_i is a velocity component ($\vec{\upsilon} = [\upsilon_1, \upsilon_2, \upsilon_3]^T$) and x_i is coordinate direction, viscous stress tensor

$$\tau_{ij} = 2\mu S_{ij} + \lambda\frac{\partial\upsilon_k}{x_k}\delta_{ij} = 2\mu S_{ij} - \left(\frac{2\mu}{3}\right)\frac{\partial\upsilon_k}{\partial x_k}\delta_{ij} \tag{11}$$

Where
$$S_{ij} = \frac{1}{2}\left(\frac{\partial\upsilon_i}{\partial x_j} + \frac{\partial\upsilon_j}{\partial x_i}\right)$$

For incompressible flow, with $\upsilon = \mu/\rho$, is being the kinematic

World Academy of Science, Engineering and Technology
International Journal of Aerospace and Mechanical Engineering
Vol:5, No:8, 2011

viscosity coefficient and ∇^2 Laplace operator.

$$\frac{\partial \upsilon_i}{\partial x_i} = 0$$

$$\frac{\partial \upsilon_i}{\partial t} + \upsilon_j \frac{\partial \upsilon_i}{\partial x_j} = -\frac{1}{\rho}\frac{\partial p}{\partial x_i} + \nu \nabla^2 \upsilon_i \qquad (12)$$

$$\frac{\partial T}{\partial t} + \upsilon_j \frac{\partial T}{\partial x_j} = k \nabla^2 T$$

Turbulence model Spalart-Allmaras one-equation model [9] employs transport equation for an eddy-viscosity variable $\overline{\upsilon}$. It was developed, based on empiricism, dimensional analysis and Galilean invariance and selected dependence on the molecular viscosity. The transport equation is expressed as

$$\frac{d\overline{\upsilon}}{dt} = \frac{1}{\rho}\left[\nabla.\left((\nu + \overline{\nu})\nabla\overline{\nu} \right) + C_{b2}(\nabla\overline{\nu})^2 \right]$$

$$+ C_{b1}(1 - f_{t2})\tilde{S}\overline{\nu} - \left[C_{w1}f_w - \frac{C_{b1}}{k^2}f_{t2} \right]\left[\frac{\overline{\nu}}{d} \right]^2 \qquad (13)$$

$$+ f_{t1}(\Delta q)^2$$

Where the eddy viscosity is given by

$$\nu_t = \overline{\nu}f_{\nu 1} \qquad \chi = \frac{\overline{\nu}}{\nu} \qquad (14)$$

The turbulent eddy viscosity is obtained from $\mu_T = f_{\nu 1}\rho\overline{\nu}$ the production term is evaluated with

$$\tilde{S} = f_{\nu 3}S + \frac{\tilde{\nu}}{\kappa^2 d^2}f_{\nu 2} \qquad (15)$$

$$f_{\nu 2} = \left(1 + \frac{\chi}{C_{\nu 2}}\right)^{-3}$$

$$f_{\nu 3} = \frac{(1 + \chi f_{\nu 1})(1 - f_{\nu 2})}{\max(\chi, 0.001)}, \chi = \frac{\tilde{\nu}}{\nu_L}$$

And S stands for the magnitude of the mean rotation rate, i.e

$$S = \sqrt{2\Omega_{ij}\Omega_{ij}} \qquad (16)$$

Where Ω_{ij} modification was suggested by Spalart

$$\Omega_{ij} = \frac{1}{2}\left(\frac{\partial \upsilon_i}{\partial x_j} - \frac{\partial \upsilon_j}{\partial x_i} \right) \qquad (17)$$

From above equations various constants are defined
C_{b1}=0.1355, $\quad C_{b2}$=0.622, $\quad C_{\upsilon 1}$=7.1, $\quad C_{\upsilon 2}$=5, $\quad \sigma$= 2/3, κ=0.41, $\quad C_{w1} = C_{b1}/\kappa^2 +(1+C_{b2})/\sigma$, $\quad C_{w2} = 0,3$, $C_{w3} = 2$, $\quad C_{t1} = 1$, $\quad C_{t2}=2$, $\quad C_{t3} = 1.3$, $\quad C_{t4} = 0.5$

The SA model in integral form after the transformation into finite-volume framework is

$$\frac{\partial}{\partial t}\int_\Omega \tilde{\nu}d\Omega + \oiint_{\partial\Omega}(F_{c,T} - F_{\nu,T})ds = \int_\Omega Q_T d\Omega \qquad (18)$$

Kω turbulence model includes two equations one for the turbulent kinetic energy k, and a second for the specific turbulent dissipation rate ω. A combination of physical processes unsteadiness, convection, diffusion, dissipation and production observed in fluid can be represent as

$$\rho\frac{\partial \omega}{\partial t} + \rho u_j \frac{\partial \omega}{\partial x_j} = -\beta\rho\omega^2 + \frac{\partial}{\partial x_j}\left[\sigma\mu_t \frac{\partial \omega}{\partial x_j} \right] \qquad (19)$$

The kω Shear Stress Transport (SST) turbulence model of Menter merges the k-ω model of Wilcox with a high Reynolds number k-ε model. SST model gives the combined positive features of both models. [10] The k-ε model is employed in the wake region of the boundary layer because the k-ω model is strongly sensitive to the free stream value of ω. The transport equations for the turbulent kinetic energy and specific dissipation of turbulence in differential form

$$\frac{\partial \rho\kappa}{\partial t} + \frac{\partial}{\partial x_i}(\rho\nu_j\kappa) = \frac{\partial}{\partial x_j}\left[(\mu_L + \sigma\kappa\mu_T)\frac{\partial \kappa}{\partial x_j} \right] \qquad (20)$$

$$+ \tau_{ij}^F S_{ij} - \beta^*\rho\omega\kappa$$

$$\frac{\partial \rho\omega}{\partial t} + \frac{\partial}{\partial x_j}(\rho\upsilon_j\omega) = \frac{\partial}{\partial x_j}\left[(\mu_L + \sigma_\omega\mu_T)\frac{\partial \omega}{\partial x_j} \right] \qquad (21)$$

$$+ \frac{C_\omega \rho}{\mu_T}\tau_{ij}^F S_{ij} - \beta^*\rho\omega^2 + 2(1 - f_1)\frac{\rho\sigma\omega^2}{\omega}\frac{\partial \kappa}{\partial x_j}\frac{\partial \omega}{\partial x_j}$$

The coefficients of the inner model (kω) are given
$\sigma_{\kappa 1}$ =0.85 $\quad\quad \sigma_\omega$=0.5 $\quad \beta_1 = 0.075$

$C\omega_1 = \beta_1/\beta^*$-$\sigma_{\omega 1}k^2/\sqrt{\beta^*}$ =0.533
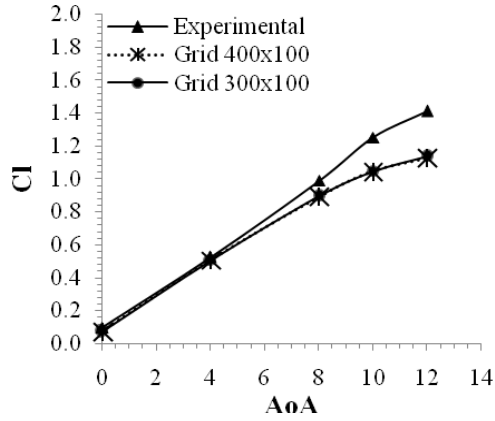
VI. RESULTS AND DISCUSSION

A. Grid Dependence Sensitivity for Clean GLC305 Airfoil

It was evaluated that grid sensitivity and optimization, for a clean GLC305 airfoil at baseline ref. experimental conditions of M = 0.12 and Re = 10.5×10^6. The grid dependence study was performed in parallel and normal directions to the airfoil surface. Four grids (300x100, 400x100, 400x200, and 400x50) were tested for this validation purpose. In all cases, the first grid point normal to the surface was at a distance of 2×10^{-4} chord length, which corresponds to a "y$^+$" of about 1 near mid-chord as
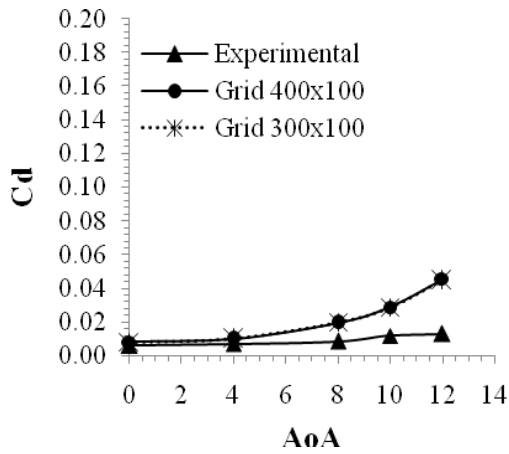
$$\Delta y = \frac{1}{\sqrt{Re}} = \frac{1}{\sqrt{10.5 \times 10^6}} = 0.0003086$$

The aerodynamic coefficients are well predicted for all the grids, except for the 400 x 50 grid. As grid points are increasing along the streamwise direction from 300 to 400 yields no notable difference for the predicted lift, drag and moment coefficients curves.
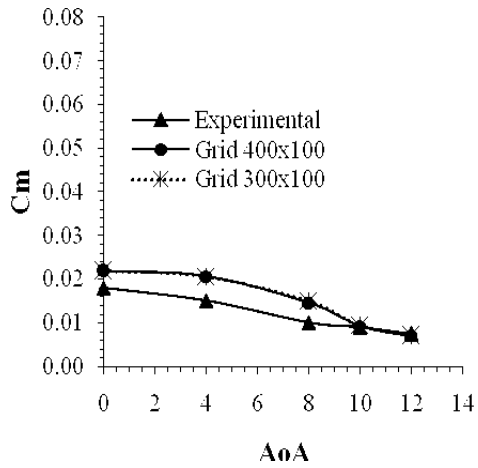
"Fig. 4" shows the lift, drag and moment coefficients for the clean GLC305 airfoil with different grid resolutions in horizontal direction of surface of airfoil, as well as the experimental results

World Academy of Science, Engineering and Technology
International Journal of Aerospace and Mechanical Engineering
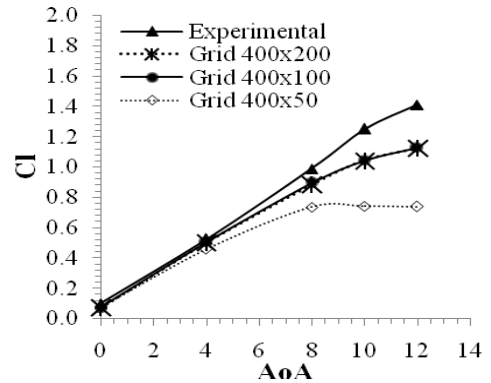Vol:5, No:8, 2011

a) Lift

b) Drag
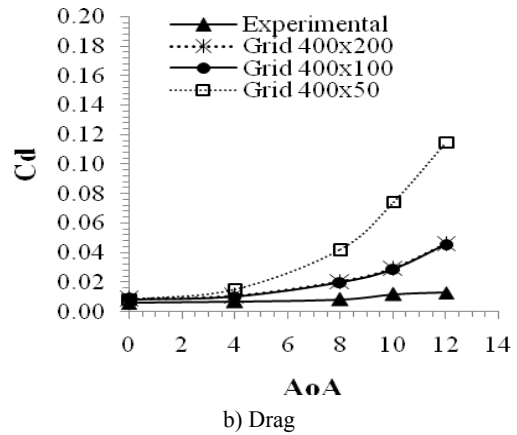

c) Pitching Moment
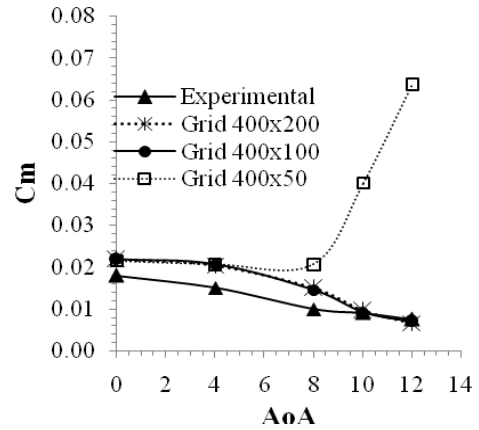Fig. 4 Streamwise Variation- Cl, Cd and Cm

grid variation take place along parallel to the surface of airfoil. At low angle of attack, computational values agree with experimental values

a) Lift

b) Drag

c) Pitching Moment
Fig.5 Normal-wise Variation- Cl, Cd and Cm

B. Turbulence Model Sensitivity for Clean GLC305 Airfoil

Navier-Stoke equation based solver has options for the turbulence model selection, including algebraic, one-equation, and two-equation models. Two turbulence models SA and Kω SST were selected to evaluate aerodynamic coefficients on clean GLC305 at M=0.12, and Re=10.5×10^6.
"Fig.6" shows that both turbulence models are good agreed at

For normal direction sensitivity, there are no significant difference between the prediction with 100 and 200 points. However, 50 grid points was found to be too coarse to describe the flow gradients and boundary layer properties, especially at higher angles of attack.
"Fig.5" shows the lift, drag and pitching moment coefficients which were evaluated for clean GLC305, when

World Academy of Science, Engineering and Technology
International Journal of Aerospace and Mechanical Engineering
Vol:5, No:8, 2011

low angle of attack with experimental results. After stall angle, SA provides the data more close to experimental as compare to SST model

a) Lift
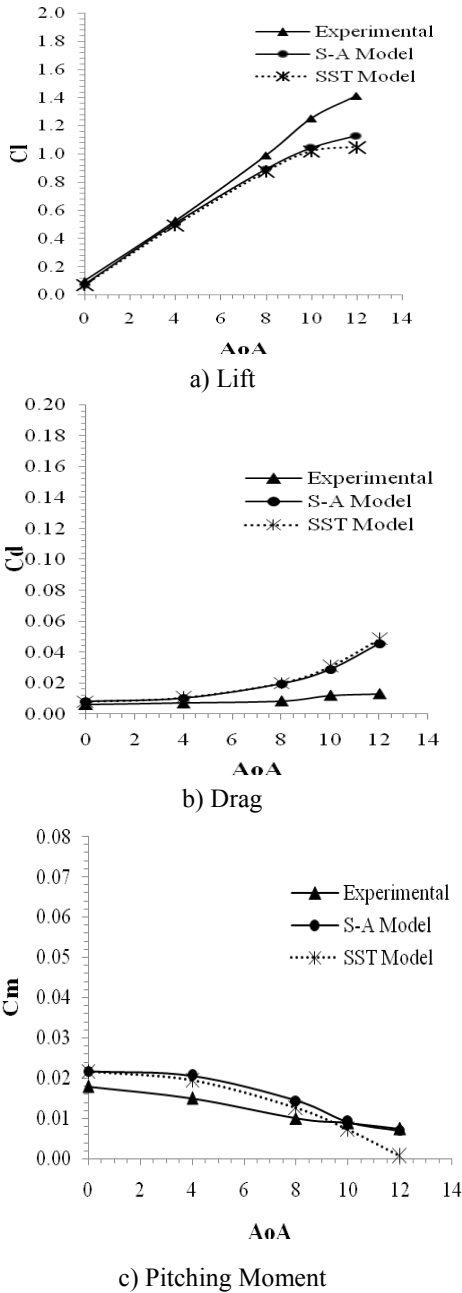

a) Lift

b) Drag

b) Drag

c) Pitching Moment

Fig.6 Turbulence Models Variation- Cl,Cd & Cm on clean GLC305 airfoil

c) Pitching Moment

Fig.7 Turbulence Models Variation on glaze 944 ice shape GLC305 airfoil

C. Turbulence Model Sensitivity for Glaze iced shape 944on GLC305 airfoil

Four turbulence models SA, Kε, Kω Std and Kω SST models are used to evaluate the aerodynamic characteristics for glaze ice shape 944 on GLC305.

"Fig.7" represents, SA, Kε and Kω SST models give the data close to each other and also good agree with experimental lift and drag coefficients values but Kω Std shows much differ. While for moment coefficient, all turbulence models are showing mixed trend.
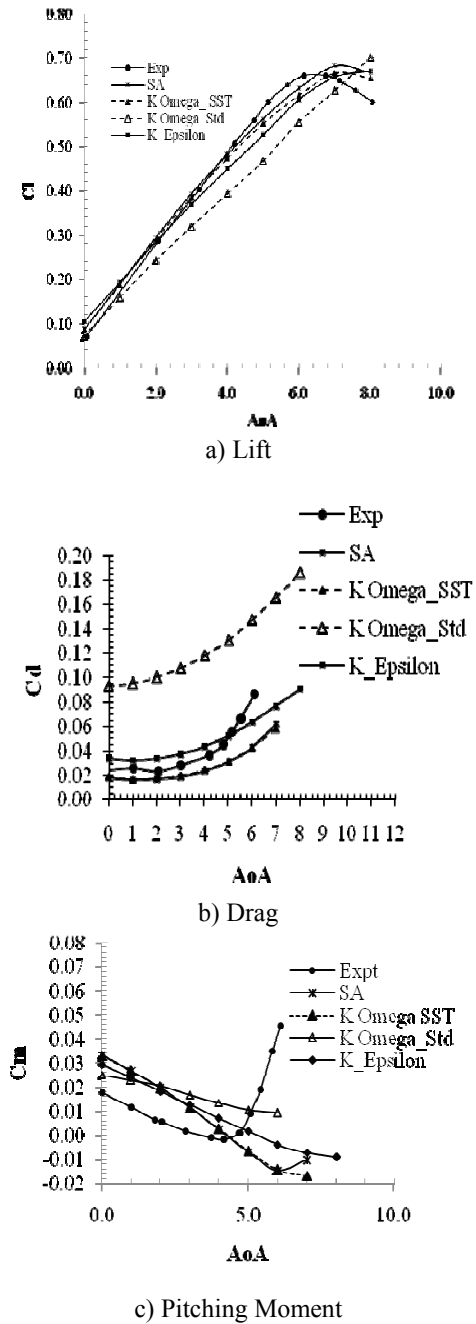
D. Effect of Mach at Fixed Reynolds Number

Aerodynamic characteristics at different Mach number 0.12, 0.21, and 0.28 on both clean and iced GLC305 airfoils were examined. 16.7 minute 212 rime ice shape is used. Numerical simulations were performed at the fixed Reynolds number at 3×10^6.   SA turbulence model was used in evaluation.

$\text{Re} = \dfrac{\rho v l}{\mu}$ where ρ v , ℓ and μ are density, velocity, reference length and dynamic viscosity respectively. At a fixed

World Academy of Science, Engineering and Technology
International Journal of Aerospace and Mechanical Engineering
Vol:5, No:8, 2011

Reynolds number but different velocity, density of medium changes as $\rho = \dfrac{\mu \mathrm{Re}}{vl}$ then $P = \rho RT$ also varies.

This study explained the compressibility behavior of airfoil aerodynamics.

"Fig.8-9" show the effect of different Mach number airflow on clean GLC305 and 212 rime iced GLC305 airfoils. Variation in aerodynamic coefficients is although small below stall angle, but its more significant after stall angle. It is also observed that at 0° up to 10° angle of attack, lift and drag coefficients have almost the same values but after 10° its behavior sudden change.

a) Lift

b) Drag
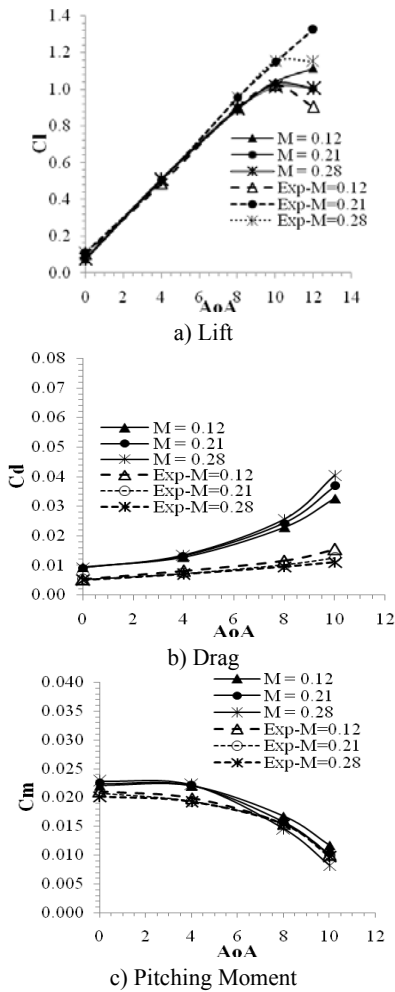
c) Pitching Moment
Fig.8 Mach number effects on Clean GLC305 Airfoil

a) Lift

b) Drag
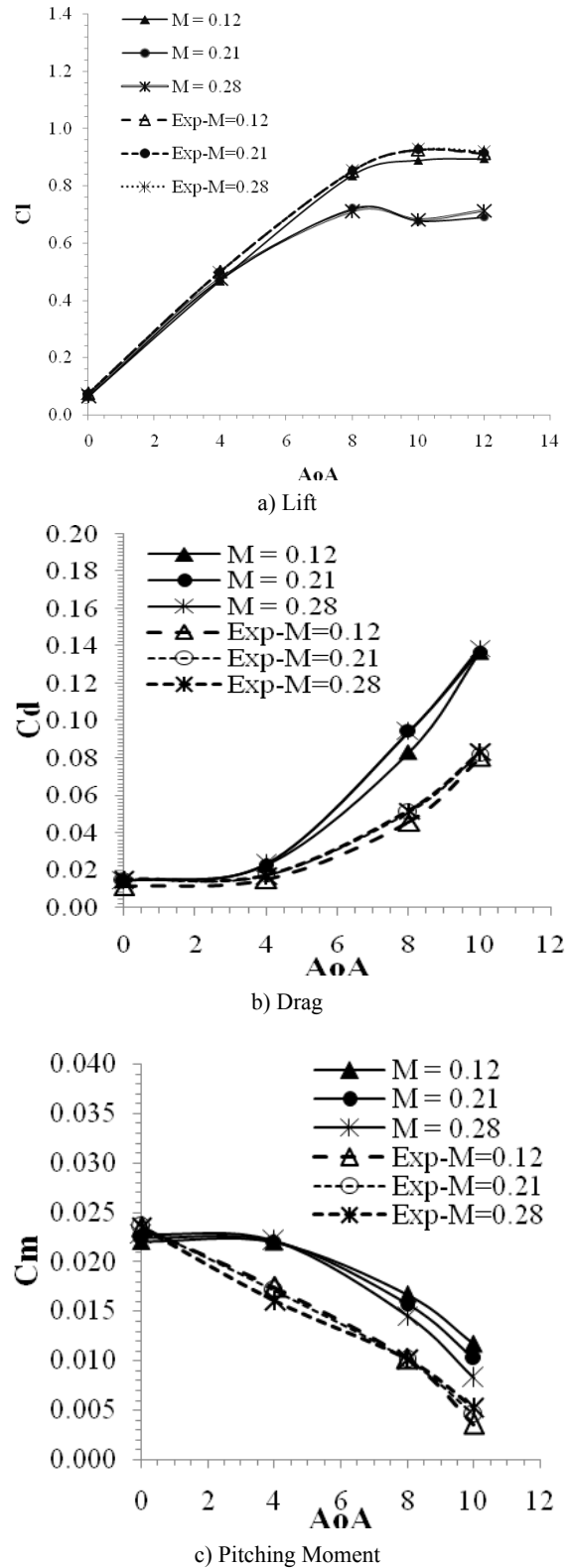
c) Pitching Moment
Fig.9 Mach number Effect on Rime GLC305 Airfoil

World Academy of Science, Engineering and Technology
International Journal of Aerospace and Mechanical Engineering
Vol:5, No:8, 2011

E. Effect of Reynolds number at Fixed Mach number

For the effect of three different Reynolds numbers 3×10^6, 6×10^6 and 10.5×10^6 at the fixed Mach number 0.12 on clean and iced GLC305 airfoils with the same configuration was examined. 16.7 minute 212 rime ice shape and SA turbulence model was used in evaluation.

"Fig.10-11" indicate that aerodynamic characteristics for clean as well as iced airfoil are almost the same at different Reynolds number but fixed Mach number.

For clean GLC305 airfoil, lift, drag and pitching moment coefficients values are much near to ref values. In iced airfoil case, pitching moment coefficient much differs from experimental values. This behavior is due to viscosity of fluid and also need much fine grid near the wall of iced airfoil.
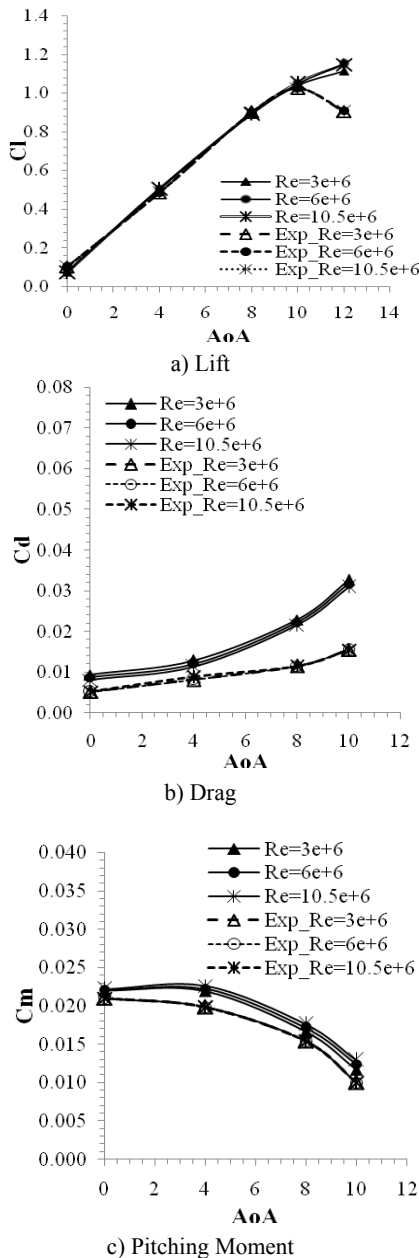

a) Lift

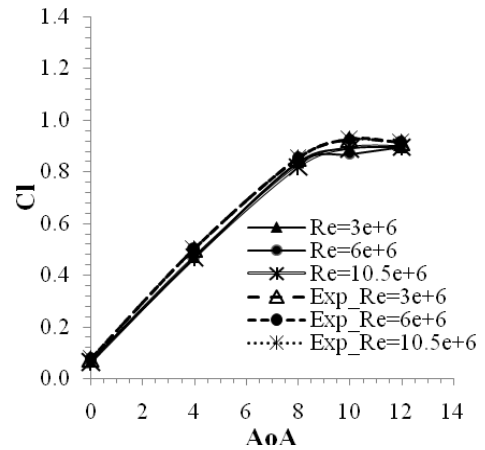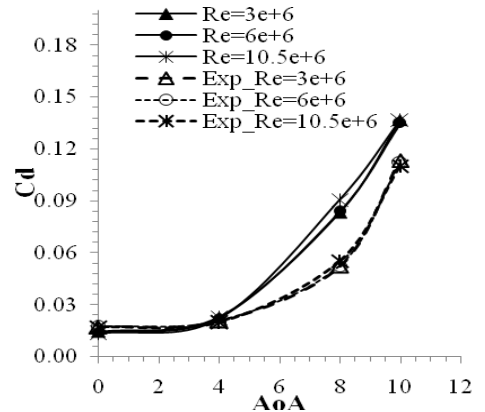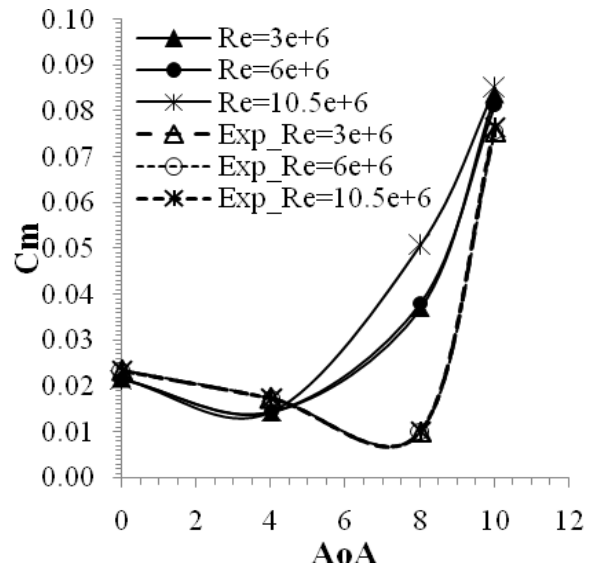

b) Drag

c) Pitching Moment

Fig.10 Effect of Reynolds number on clean GLC305 airfoil

a) Lift

b) Drag

c) Pitching Moment

Fig 11 Effect of Reynolds number on rime 212 iced GLC305 airfoil

F. Pressure distribution on iced GLC305 airfoil

The effect of turbulence models were also analyzed by considering pressure distribution on glaze ice 944 airfoil. "Fig.

World Academy of Science, Engineering and Technology
International Journal of Aerospace and Mechanical Engineering
Vol:5, No:8, 2011

12-14" show the pressure distribution at α=5°, M=0.12 by using SA, Kε, and Kω SST turbulence models

Fig. 12 Pressure distribution due to SA model
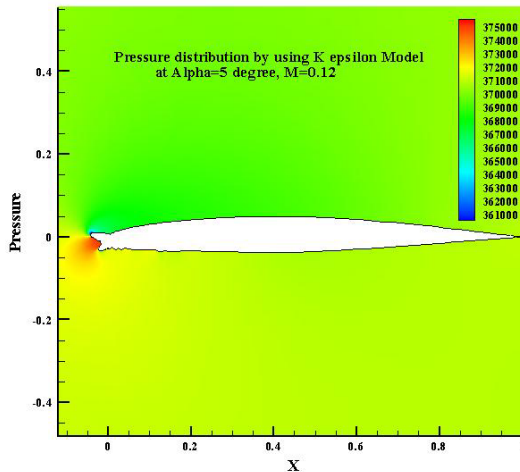
Fig. 13 Pressure distribution due to kε model
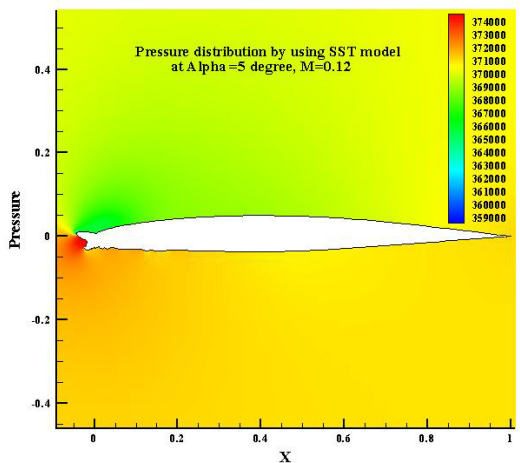
Fig. 14 Pressure distribution due to SST model

VII. CONCLUSION

In this study more than hundred cases were simulated on clean and iced GLC305 airfoil. It was observed that turbulence models SA is more effective than SST, kε, and kω standard models in calculating flow fields around clean and iced airfoil GLC305 and also represent the closest solution of experimental data.

When Reynolds number is fixed and Mach numbers varies, then values of lift coefficient and drag coefficients for rime212, glaze944 iced airfoils GLC305 are all most the same for either mach 0.12, 0.21 or 0.28. But pitching moment is slightly differ at higher AoA. When Mach number is fixed and Reynolds numbers are varies, then lift coefficient 'Cl' is approximately the same for all Re values. Cd and Cm show some differences.
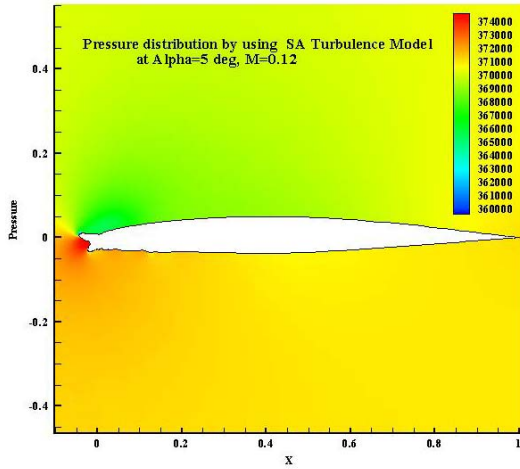
REFERENCES

[1] Kevin R. Petty* and Carol D. J. Floyd National Transportation Safety Board, Washington, DC.
[2] Chi, X., Zhu, B.Shih, T.I-P., Slater, J.W., Addy, H.E., and Choo, Y.K., "Computing Aerodynamic Performance of 2D Iced Airfoils" Blocking Topology and Grid Generation." AIAA Paper 2002-0381, January 2002
[3] Addy, H.E, "Iced Accretions and Icing Effects for Modern Airfoils", NASA/TP-2000-210031, April 2000
[4] Addy, H.E., " A Wind Tunel Study of Icing Effects on a Business Jet Airfoil" NASA/TM-2003-212124, AIAA Paper 2003-0727, February 2003 Lax, P.D. " Weak Solution of Nonlinear Hyperbolic Equation and their Numerical Computation" Comm. Pure and Applied Mathematics, 7(1954), pp.159-193
[5] Zierep,J.: Vorlesungen uber theoretische Gasdynamik(Lectures on Theoretical Gas Dynamics). G.Braun Verlag, Karlaruhe, 1963
[6] Liepmann, HG.W.; Roshko, A. "Elements of Gas Dynamics". John Wiley & Sons, New York, 1957
[7] Bertin. John J. "Aerodynamics for engineers" 2nd ed. TL570.B42 1989, ISBN 0-13-01843-
[8] Spalart, S.R.; Allmaras, S.A. "A One-Equation Turbulence Model for Aerodynamic Flows". AIAA Paper 92-0439, 1992; also in La Recherche Aerospatiale, 1 (1994), pp. 5-21
[9] Menter, F.R. "Two–Equation Eddy-Viscosity Turbulence Models for Eingeering Applications" AIAA paper 93-2906, 1993; also AIAA Journal, 32(1994), pp.1598-1605